This article has been accepted for publication in a future issue of this journal, but has not been fully edited. Content may change prior to final publication. Citation information: DOI 10.1109/JSEN.2019.2926189, IEEE Sensors Journal

A Low Power 5.8-GHz ISM-Band Intermodulation Radar System for Target Motion Discrimination

Ashish Mishra, *Student Member, IEEE*, Changzhi Li, *Senior Member, IEEE*

***Abstract* — This paper discusses the design and test of an intermodulation radar receiver and a nonlinear tag operating in the 5.8-GHz industrial, scientific, and medical (ISM) band. To discriminate reflections of the target-generated 3rd-order intermodulation frequencies from the clutter-reflected fundamental tones, the receiver was designed to attenuate the fundamental reflections and amplify the lower 3rd-order tone generated by the nonlinear target. The nonlinear tag was designed on a flexible substrate for wearable applications. Experiments were performed with two types of targets, i.e. the nonlinear tag and a metal reflector. Various experiments were performed to demonstrate the clutter rejection capability of the radar i.e. mechanical motion and vital sign detection of a human target in the presence of multiple clutter. Four experiments were recorded and analyzed in this paper. The results were recorded and analyzed to demonstrate the clutter noise rejection capability of the intermodulation radar.**

***Index Terms*— clutter rejection, intermodulation, nonlinear tag, nonlinear radar, vital signs.**

I. Introduction

Recently there have been a lot of developments in CW radars. These radars can track millimeter and even sub-millimeter displacement [1,2]. However, these conventional CW radars cannot differentiate clutter motion from target motion without prior or post modifications. Either they require specialized hardware setup and pre-calibration as in [3], which also have limitations on the number of clutter sources, or software-based approaches like cyclostationary [4], curve-fitting [5], and wavelet transform [6] algorithms which are not real time.

To differentiate multiple clutter objects from the target in real-time without specialized hardware and pre-calibration, nonlinear radars are used [7-11]. These radars are based on the nonlinear characteristics present in many electronic components such as diodes and transistors. Since naturally occurring things are mostly linear in behavior with exceptions such as the rusty bolt effect, they can be distinguished from the nonlinear components which are man-made. The rusty bolt effect and passive intermodulation can be a source of interference at high power levels around 40 dBm [12, 13]. The nonlinear scattering of an antenna with nonlinear load is modeled using Volterra series and time domain analysis is performed and discussed in [14, 15]. In nonlinear radars, fundamental tone(s) is sent towards a nonlinear tag, which in return reflects nonlinear tone(s) along with the fundamental tone(s). In the receivers, the fundamental tone(s) is separated from the nonlinear response to distinguish between targets and clutter [7-11].

Nonlinear radars commonly used, work on the detection of harmonics of the transmitted tone(s), which lead to some major challenges in design, e.g., radio spectrum licensing issues [10], and the high path loss of the harmonic tones compared with the fundamental tone(s) as per free space path loss model. Whereas in this paper, intermodulation responses from the nonlinear devices were utilized for clutter rejection purposes. The intermodulation response has some benefits over the harmonic response. For instance, the intermodulation response lies in the same band as the fundamental tones, so they have almost the same path loss as the fundamental tones while the 2nd-order harmonic response suffers from 6 dB more path loss than the fundamental response. So, if the same power is assumed to be reflected from a 2nd-order harmonic tag and an intermodulation tag, the power at the radar receiver will be more for the intermodulation response as compared to the harmonic response. Since harmonic frequency tones are widely separated from the fundamental tones, many harmonic radars need two different kinds of devices for radar transmitter and receiver chains. The same is also true for tags, where two different antennas are needed. This increases the tag size. While in the case of intermodulation radar, the nonlinear and fundamental responses are in the same band, so a single antenna can perform the roles of both receiving and transmitting. As compared to [16], the radar was able to suppress the clutter motion for the same amplitude motion, but in this work, a large clutter motion was suppressed as compared to tag motion. In [17], an active tag was used as a frequency doubler. The active tag is noisy compared to the passive tag and requires regular battery replacement. Similarly, the sub-harmonic radars in [18] used active tags. They have reduced path loss at the cost of increased receiver size. Both the harmonic and subharmonic radars suffer from licensing issues and require two different antennas or dual-band antennas to function as the transmitter and receiver. Active backscatter-based radars send out a frequency tone at f_1 and have a tag transmitting signal at f_m , so the received signal gets modulated and there is a frequency shift of $f_1 \pm f_m$. The tags for these radars need an oscillator to send out a frequency tone and are different from the tags of harmonic or sub-harmonic radars where the nonlinear property of the tag

Manuscript was submitted for review on March 23, 2019; revised on May 31, 2019; revised on June 21, 2019. The authors would like to acknowledge grant support from National Science Foundation (NSF) ECCS-1808613 and CNS-1718483.

A. Mishra and C. Li are with the Department of Electrical & Computer Engineering, Texas Tech University, Lubbock, TX 79409, USA. (email: ashish.mishra@ttu.edu; changzhi.li@ttu.edu)

This article has been accepted for publication in a future issue of this journal, but has not been fully edited. Content may change prior to final publication. Citation information: DOI 10.1109/JSEN.2019.2926189, IEEE Sensors Journal

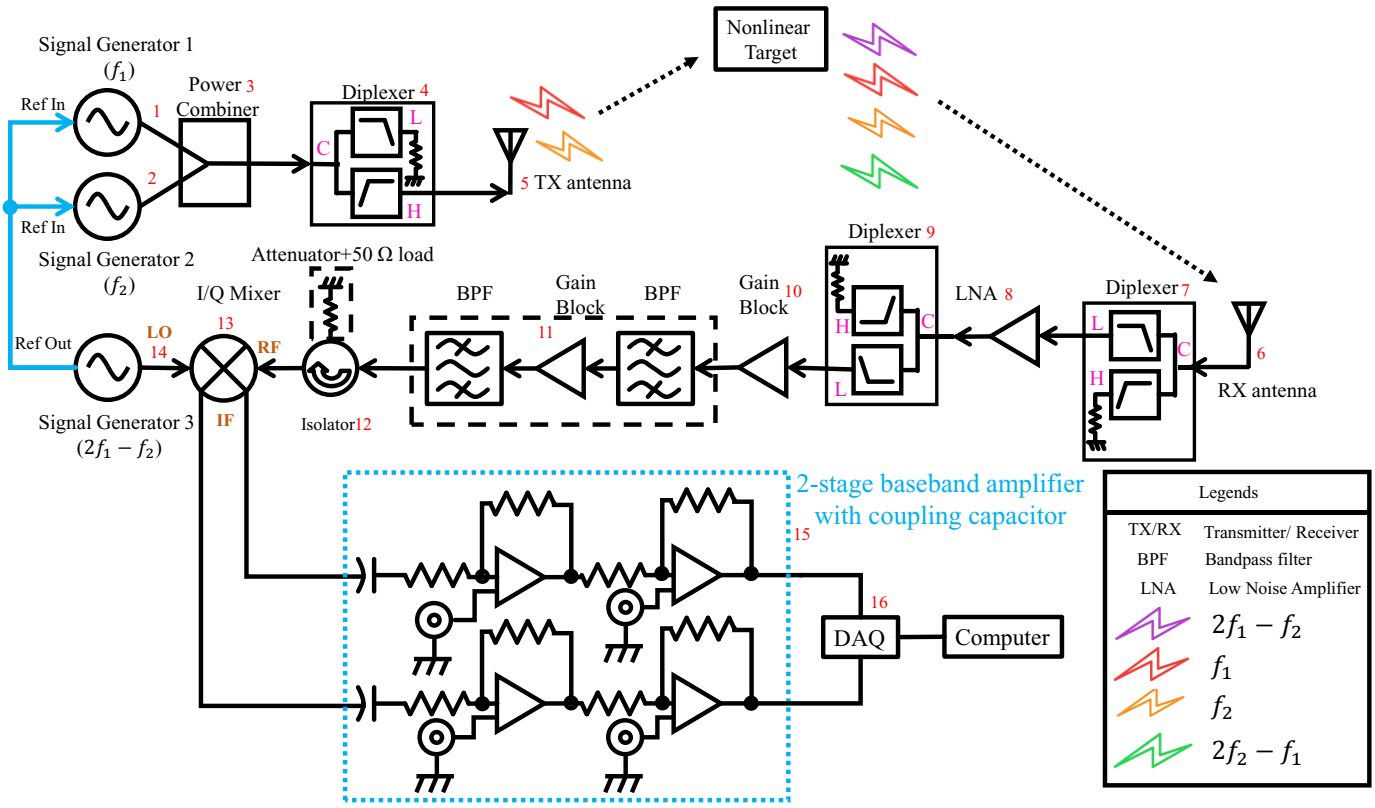

Fig. 1. The 5.8-GHz ISM-band intermodulation radar and its non-linear target.

generates additional tones and not by the oscillator. Active backscatter-based radars i.e. radar having tags which act as a frequency modulator for target localization have noisy tags [19] and require amplifiers and oscillators, making it costly and power hungry. These active tags cannot be sealed to reduce wear and tear as they require frequent battery replacement to supply power [20]. Table 1 summarizes the three nonlinear radars and their characteristics.

In this paper, a new nonlinear radar is designed based on the principle of intermodulation to separate clutter from the target of interest. This intermodulation radar can overcome some drawbacks of harmonic radars. Its 3rd-order tones are close to the fundamental tones, sharing almost the same path loss as the fundamental tones while, the harmonic radar requires its nonlinear target to operate in two largely separated frequency bands. Also, the same antenna can be used as both the receiver and the transmitter in the tag. [21]. Compared with active backscatter-based radar, the proposed tag does not require any power supply and has a reduced number of RF components, simplifying the tag design and eliminating the battery life issue.

By studying the drawbacks suffered by the existing radars, a new radar was designed to overcome their existing issues. The radar operates in the 5.8-GHz-ISM band with fundamental tones at 5.79 GHz and 5.84 GHz, respectively. The 3rd-order response at 5.74 GHz generated by the tag is utilized to differentiate the target from clutter. The radar works at a 5 V supply voltage and has a power consumption of approximately 3.25 W. In the previous work [10], the radar was able to detect approximately 2 cm motion up to 0.5 m distance. The sensitivity of the radar was around -65 dBm. The tag was made on a nonflexible substrate, making it difficult to perform vital signs measurement of a human target. In this work, the theoretical sensitivity was improved to around -120 dBm. The detection range and the minimum detectable motion by the radar were also improved. The new tag was fabricated on a flexible substrate so that a human target can wear it. The potential applications for this radar include vital sign monitoring in health care, device identification and rescue operation.

This paper is arranged into four sections. Section II discusses the theory and design of the intermodulation radar and passive nonlinear tag. Section III presents the measurement results. A conclusion is drawn in Section IV.

II. Intermodulation Theory and Receiver Design

When two frequency tones f_1 and f_2 ($f_1 < f_2$) interact with a nonlinear device, additional frequency tones are generated at $mf_1 \pm nf_2$, where m and n could be any integer numbers. The lower 3rd-order tone $f_{r1} = 2f_1 - f_2$ was used in this radar as it is close in frequency to the fundamental frequency tones and has lower path loss than other frequency tones.

A. Radar system

Fig. 1 shows the complete block diagram of the intermodulation radar. The part numbers labeled in Fig.1 in red correspond to the blocks shown in Fig. 2. The radar transmits fundamental tones at approximately 5 dBm power level and receives two additional tones f_{r1} and f_{r2} ($f_{r2} = 2f_2 - f_1$) in addition to f_1 and f_2 at the receiver. The f_1, f_2 and f_{r2} tones were attenuated by the diplexers in the receiver path and thus can be ignored. To maintain coherence and achieve the required sensitivity based on the range correlation effect [21], all three

This article has been accepted for publication in a future issue of this journal, but has not been fully edited. Content may change prior to final publication. Citation information: DOI 10.1109/JSEN.2019.2926189, IEEE Sensors Journal

TABLE 1: NONLINEAR RADAR TYPES AND SPECS

Radar / Specs	Intermodulation	Harmonic	Sub-Harmonic
Licensing Issue	No	Yes	Yes
Nonlinear response	$2f_1 - f_2$, $2f_1 - f_2$ etc.	$2f, 3f, 4f$ etc	$f/2, f/4$ etc.
Antenna	Single band	Dual band	Dual band
Path loss	Same as fundamental	At least 6dB more than fundamental	At least 6dB less than fundamental
Tag type	Passive/Active	Passive/Active	Active
Tag design	Matching circuit for 1 band only	Matching circuit for 2 band	N/A
Lifetime	Tag wear and tear (Passive)	Tag wear and tear (Passive)	Battery life
Components needed	Diode, match circuit and single band antenna	Diode, match circuit and dual band antenna	Dual band antenna, frequency divider and battery

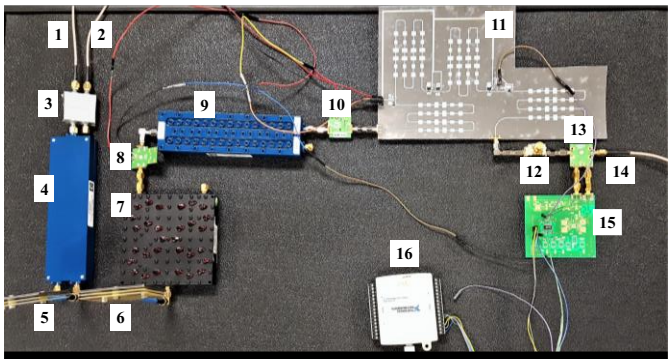

1: From SG1; 2: From SG2; 3: Power combiner; 4: Diplexer; 5: TX antenna; 6: RX antenna; 7: Diplexer; 8: LNA; 9: Diplexer; 10: Gain block; 11: Gain block and filter board; 12: Isolator; 13: I/Q mixer; 14: From SG3; 15: Baseband amplifier; 16: DAQ

Fig. 2. Intermodulation radar setup.

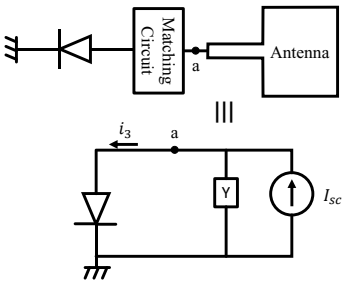

Fig. 3. Nonlinearly loaded antenna (tag) and equivalent circuit.

signal generators share the same reference, which is provided by signal generator 3 (SG3). Two fundamental tones of equal amplitudes, which were generated using signal generator 1 (SG1) and signal generator 2 (SG2), are fed to the transmitting antenna through the power combiner and high frequency path of the diplexer. The use of a diplexer was important in the transmitter as it helped in attenuating any 3rd-order intermodulation tones, which might be generated due to passive devices, such as the power combiner or a reflection from the power combiner to the signal generator. The pass band of the high frequency path of the diplexer is from 5.78GHz to 5.84GHz and provides attenuation of 75 dB for out-of-band signals. The two transmitted tones are denoted as

$$T(t) = \sum_{i=1}^{2} \cos[2\pi f_i t + \phi_i(t)] \quad (1)$$

where $\phi_i(t)$ is the phase noise of the two signal generators.

The nonlinear tag used in this project was passive and had Schottky diodes to generate a nonlinear response. As a result, the radar received signal can be expressed as

$$R(t) = \cos\left[2\pi f_{r1} t - \frac{4\pi x_o}{\lambda} - \frac{4\pi x(t)}{\lambda} - \phi\left(t - \frac{2x_o}{c}\right)\right] \quad (2)$$

In (2), λ is the wavelength corresponding to f_{r1}, $x(t)$ was the mechanical displacement of the target, x_o was the nominal distance between the target and the radar, and the signal amplitude is normalized to one. The fundamental components, the higher 3rd-order component f_{r2}, and the other nonlinear tones were ignored in (2) as they are attenuated. Again, the diplexer attenuates out-of-band tones by 75 dB while passing frequency tones from 5.72-GHz to 5.75-GHz in the low frequency path. The received signal was amplified by the LNA and passed through the diplexer again to further attenuate any out-of-band tones generated due to the LNA. The two diplexers are not connected sequentially, to lower the noise figure (NF) of the system, as attenuation by the diplexer in the pass band increases the NF of the system. The signal was further amplified and sent to the RF port of the mixer. Apart from attenuating the fundamental tone(s), the isolation was also a key criterion for the receiver design, because the leakage from the local oscillator (LO) port to the radio frequency (RF) port can radiate back to the surroundings. Because of this, the corresponding clutter reflection can be comparable to the 3rd-order tone generated by the tag, leading to clutter interference. The reverse isolation from the mixer RF port to the RX antenna port was designed to be above 50 dB across the 5 to 6 GHz band.

The local oscillator (LO) port of the mixer was driven by a signal with a frequency f_{r1}, which also provided additional rejection of other frequency tones. The data acquisition device (DAQ) used was the NI-USB 6009 with a maximum sampling frequency around 48-KHz. Down converting with f_{r1}, the response of the f_1 and f_2 tones were 50-MHz and 100-MHz from that of the f_{r1} tone, which was beyond the processing speed of the DAQ and hence were largely attenuated.

The radar was AC-coupled at the mixer output to remove the DC offset. The baseband amplifiers had a bias of 2.5 V, which was halfway between the two supply rails of 0 V and 5V and were implemented in an inverting amplification configuration. The *I* and *Q* channel output signals from the baseband amplifier can be expressed as

$$B_{I/Q}(t) = A_{I/Q}\cos\left[\theta + \frac{4\pi x(t)}{\lambda} + \Delta\phi(t)\right] \quad (3)$$

This article has been accepted for publication in a future issue of this journal, but has not been fully edited. Content may change prior to final publication. Citation information: DOI 10.1109/JSEN.2019.2926189, IEEE Sensors Journal

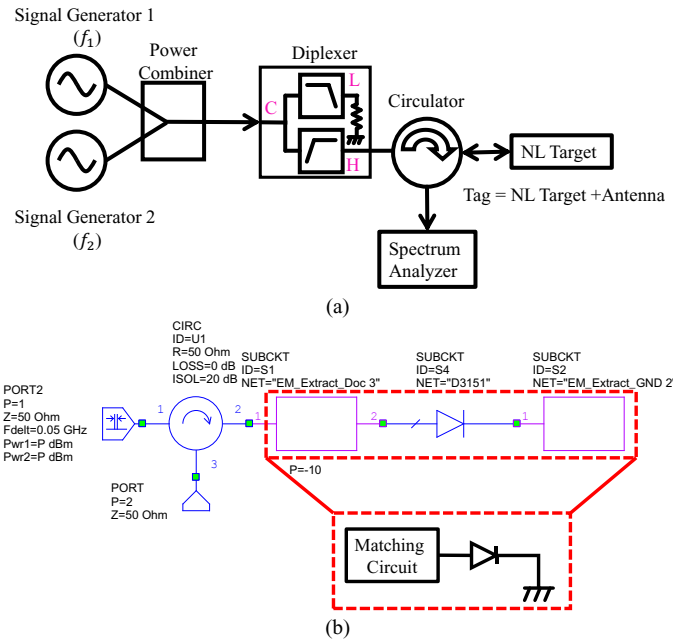

Fig. 4. Conversion loss of the nonlinear tag: (a) Measurement setup (b) Simulation setup.

where $\theta = \frac{4\pi x_o}{\lambda} + \theta_o$. θ_o accounts for the phase shift when the signal is reflected from the tag and propagates along building blocks in the radar signal chain. $\Delta\phi(t)$ is the residual phase noise, which can be ignored for short range detection due to the range correlation effect [22]. A_I and A_Q are the amplitudes of the *I/Q* channel baseband outputs. The use of *I/Q* channels solves the null detection point issue [22]. These baseband signals are converted from analog to digital using the DAQ. Zero padding was then added to the data to get the true peak of the motion when using a Fast Fourier Transform (FFT) in MATLAB. The FFT data was symmetrical about 0-Hz. Hence, the positive frequencies of frequency domain data were plotted as it contains all the motion information.

Fig. 2 shows the top view of the transmitter and receiver of the radar. SG1 and SG2 are the signal generators connected to the transmitter and operate at 5.79-GHz and 5.84-GHz, respectively. SG3 is the signal generator at 5.74-GHz connected to the LO port of the mixer. The isolator labeled as part 12 in Fig. 2 was realized by a circulator, connecting port 1 as an input, port 2 to the RF port of the mixer, and port 3 to a 50 Ω load. The reverse isolation from port 2 to port 1 was around 20 dB. The loading of the circulator has been improved using an extra attenuator to improve the isolation.

B. Nonlinear tag

The passive nonlinear tag was designed for operation without requiring any battery. Infineon's BAT 15-03W Schottky diode was used in the tag design. The S-parameter model of the diode with 0-V and 0-mA bias was used in the design of the microstrip line matching circuit for each unit cell. A 5.8-GHz ISM-band patch antenna was also integrated into each unit cell. The tag contains a 4×9 array of unit cells. The same antenna works as a receiving antenna for fundamental tones and as a transmitting antenna for the nonlinear reflection response of the diode.

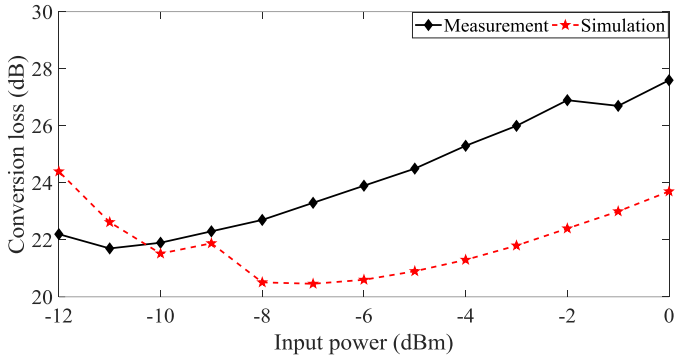

Fig. 5. Measured and simulated conversion loss from f_1 to f_{r1} on the nonlinear tag.

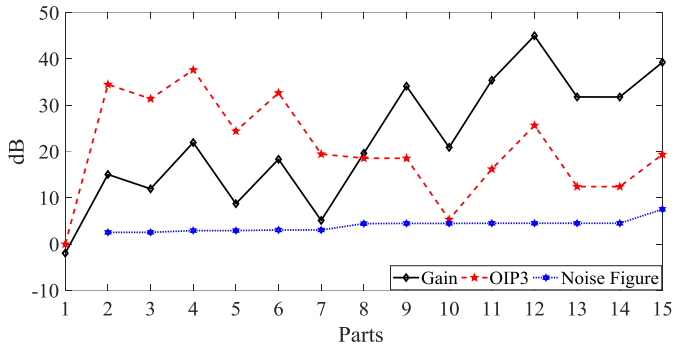

1: Diplexer (7); 2: LNA(8); 3: Diplexer(9); 4: Gain Block(10); 5-13: Gain Block and filter board(11); 14: Circulator(12); 15: *I/Q* Mixer(13)

"A:B(C)" means A: Part in graph; B: Name; C: Corresponding part in Fig. 2

Fig. 6. RF link budget of the receiver.

The nonlinearly loaded antenna is shown in Fig. 3. The tag was placed in the radiation region of the transmitting antenna of the radar. The radiation patterns generated by the TX antenna of the radar contains E-field information at f_1 and f_2. The summation of E-fields parallel to the patch antenna along the broadside direction is denoted as E_i. The I_{sc} in Fig. 3 is the short circuit generated due to E_i and Y is the linear admittance. I_{sc} is directly proportional to E_i. The nonlinear property of the diode generates the 3rd-order tone, along with higher order tones, in addition to the fundamental. In this paper, the discussion was limited to 3rd-order tones only. The 3rd-order and fundamentals were backscattered by the same antenna. These backscattered frequencies were sent towards the receiving antenna of the radar. Two different antennas were used on the radar side, i.e. one as the transmitting antenna and the second as the receiving antenna to reduce coupling and leakage from the transmitter to the receiver.

C. Fundamental-to-3rd-order conversion loss

Fig. 4(a) shows the setup of measuring the nonlinear target's conversion loss from the fundamental to the 3rd-order tone. The two fundamental tones at f_1 and f_2 are fed to the power combiner. The output of the power combiner was sent to the high frequency path of the diplexer. The high frequency path offers an attenuation of 3 dB in the pass band and 75 dB for out-of-band frequencies. The frequencies at f_{r1} and f_{r2} fall in the out-of-band of the high frequency path of the diplexer. The purpose of the diplexer was to attenuate the 3rd-order tone that might be generated due to passive intermodulation from the

This article has been accepted for publication in a future issue of this journal, but has not been fully edited. Content may change prior to final publication. Citation information: DOI 10.1109/JSEN.2019.2926189, IEEE Sensors Journal

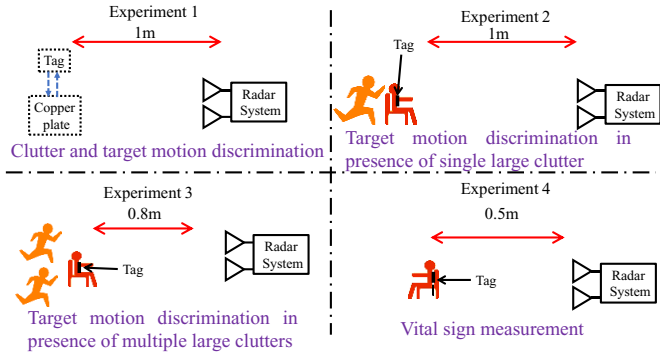

Fig. 7. Various experiments performed.

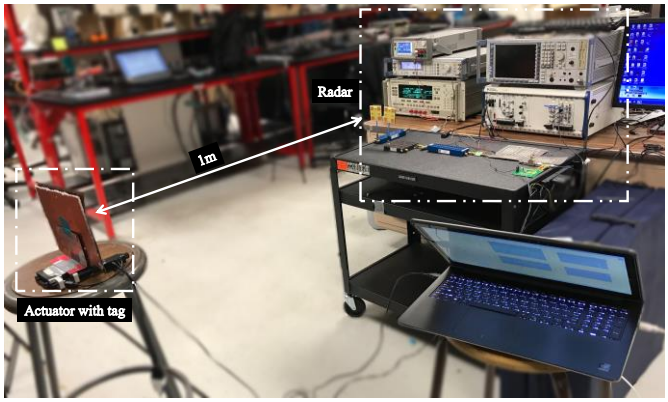

Fig. 8. Experiment 1 setup.

power combiner or reflection from the power combiner towards the signal generator [23]. The output of the diplexer was sent towards the circulator's port 1. The nonlinear target was connected to port 2 of the circulator, while the output from the nonlinear target was sent to port 3 of the circulator, which in turn was connected to the spectrum analyzer for measurement of the 3rd- order tone at f_{r1}. The input power of f_1 and f_2 tones sent towards the tag was swept from 0 dBm to -12 dBm, and the f_{r1} response generated by the tag was measured. The conversion loss was calculated as the difference in the power level of the input of the f_1 tone from the f_{r1}tone. The cable loss was considered while measuring the power of the 3rd-order and fundamental tones and the signal generators were also calibrated for each power level of the fundamental tones. Fig. 5 shows the conversion loss of the tag as a function of the input power. The minimum conversion loss was approximately 22 dB with -11 dBm input power. Further reducing the input power, the conversion loss increases as 3rd-order tone power level reduces.

In this radar, both the transmitting and receiving antennas have a gain of 14 dB. The tag has an antenna array of 36 elements. The total gain of the 36-element antenna array was around 19 dB. Since frequencies 5.79 GHz and 5.84 GHz are close to each other, the wavelength is assumed equal for 5.79 GHz and 5.84 GHz. For the calculation, the wavelength was taken as 0.0517 m. The path loss was around 14.7 dB (~15 dB) for 1 m distance as per free space path loss model. The power available to the nonlinear tag at 1 m distance would be approximately -10 dBm. The conversion loss for an input power of -10 dBm was about 22 dB. Hence, the measurements and

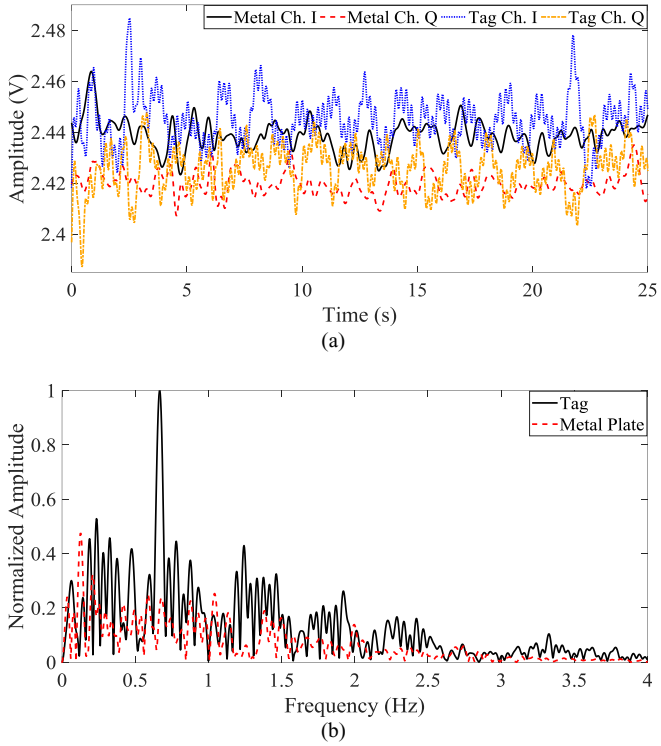

Fig. 9. Nonlinear tag vs. metal plate: (a) Baseband output for metal and nonlinear tag motion (b) FFT of baseband signal.

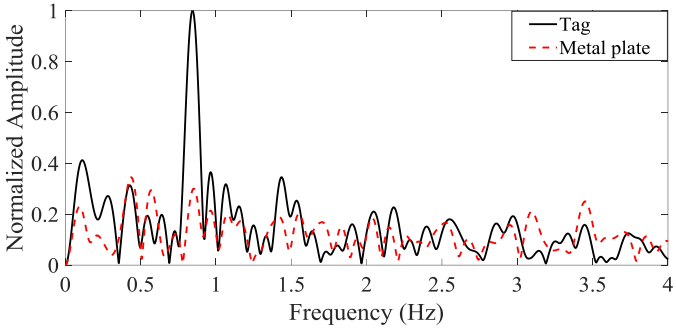

Fig. 10. FFT spectrum for 1mm amplitude at 0.9 Hz.

simulation were performed up to -12 dBm input power as shown in Fig. 5.

The measured conversion loss was compared with the simulation results. To measure the nonlinear response of the diode, the S-parameter model used in the design of the matching circuit was replaced by the Spice model provided by the manufacturer. National Instrument's AWR software was used in the design and simulation of the tag. The simulation setup to measure 3rd-order tones is shown in Fig. 4(b). Two tones f_1 and f_2 were sent by the 2-tone harmonic balance port towards the input of the nonlinear target through the circulator from port1 to port 2 and the nonlinear response was read out at port 3 of the circulator. Similarly, as in the measurement setup, the conversion loss was calculated in the simulation setup as the difference between the power input at the f_1 tone and the nonlinear response at the f_{r1} tone. The conversion loss measured due to the simulation was plotted in Fig. 5. By comparing the simulation and measured conversion loss, the conversion loss difference was almost less than 1 dB for input

This article has been accepted for publication in a future issue of this journal, but has not been fully edited. Content may change prior to final publication. Citation information: DOI 10.1109/JSEN.2019.2926189, IEEE Sensors Journal

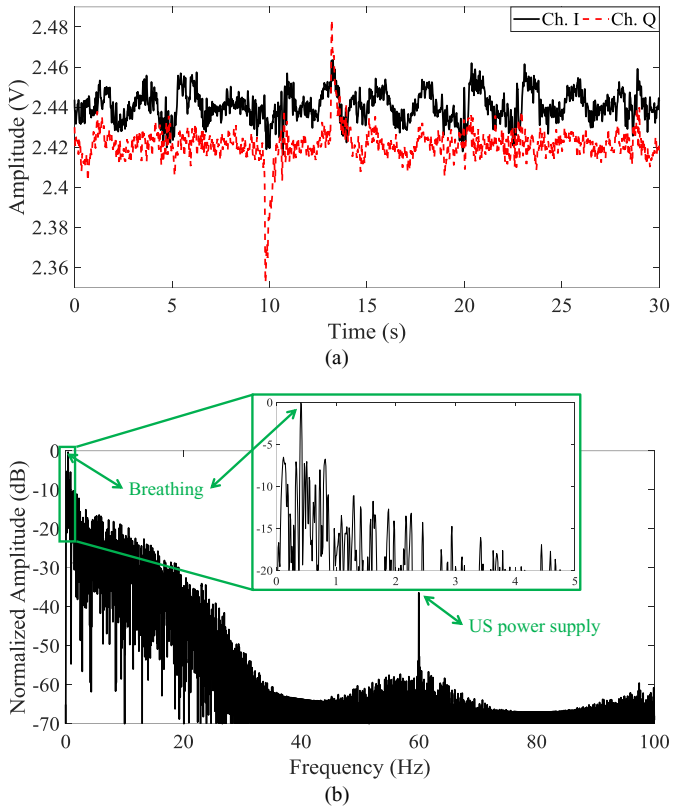

Fig. 11. Target detection in the presence of single clutter object: (a) Baseband output for tag and single clutter simultaneous motion (b) FFT of baseband signal.

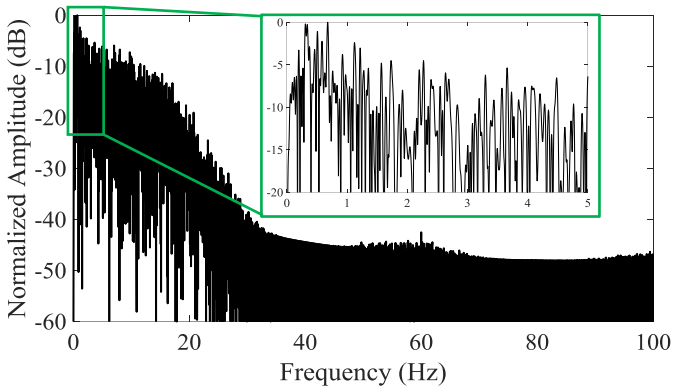

Fig. 12. FFT spectrum in presence of single clutter object and no tag.

power from -9 dBm to -11 dBm input power. Since the nonlinear target becomes saturated above -5 dBm input power, the 3rd-order response does not increase as input power to the device increases.

D. Radar Link Budget Analysis

The radar link budget analysis was performed. The radar receiver was simulated in the NI-AWR software from part number 7 to 14 in Fig. 2 and the noise figure (NF), gain (G) and output referred third-order intercept point (OIP3) were plotted in Fig. 6 for frequency 5.74 GHz. The parameters were based on those from manufacturer datasheets whenever available. Otherwise estimated parameters were used based on typical performance in the operating frequency and power range.

III. System Level Experiment

Four types of experiments were performed. Fig. 7 shows an overview of the four experiments.

- In experiment 1, the mechanical motion of equal amplitude was used to differentiate tag and clutter motion, while in experiment 2 and experiment 3, clutter motion was stronger than tag motion.
- For experiment 1, two types of targets were used, i.e. the fabricated nonlinear tag with a size of 26.67 cm×19.56 cm corresponding to a radar cross section (RCS) of 12.9 m^2 and a copper plate (metal plate) with a size of 30.48 cm×22.86 cm corresponding to an RCS of 22.7 m^2. The copper plate was used to mimic an undesired clutter with a size larger than the nonlinear tag. The RCS values reported is based on $\sigma = \frac{4\pi b^2 l^2}{\lambda^2}$ where b, l are dimensions of the tag and copper plate and λ is the wavelength at 5.8 GHz. The RCS calculated by the above equation reports the maximum RCS value for the given dimension of a flat plate.
- A computer-controlled actuator, which can generate the desired movement amplitude and frequency, was used to generate mechanical movements for experiment 1.
- In experiment 2, person 1 wearing the tag was sitting in front of the radar and clutter motion from person 2 was generated around person 1.
- Additional clutter was introduced by adding person 3 to generate clutter motion in experiment 3.
- Experiment 4 was for vital sign measurement where person 1 was wearing the tag on the back of the body and measurements were recorded. The measurement from the back side increases the chance of recording the heartbeat of a person.
- The measurements for experiments 1 and 2 were recorded with the targets placed 1 m away from the intermodulation radar, while experiment 3 was measured at 0.8 m from radar and in experiment 4, vital sign measurement was performed at 0.5 m away from the radar.

A. Nonlinear Tag vs. Copper Plate

The measurement setup of experiment 1 is shown in Fig. 8. The experiments were performed in a typical lab environment with furniture and other clutter scattered around the radar.

In this experiment, the nonlinear tag and copper plate were mounted in successive tests on the actuator moving with 0.5 mm peak-to-peak amplitude and 0.7-Hz frequency in front of the radar. The baseband data was recorded at 20 Hz sampling frequency using NI-USB 6009 and an FFT was performed. The results are shown in Fig. 9. From this graph, it can be seen that the signal detected from the nonlinear tag had a peak at 0.7-Hz while the peak from the copper plate at 0.7-Hz was of the same level as noise and showed a random peak at 0.2-Hz, despite the copper plate having a larger physical size than the nonlinear tag. The experiment was repeated for a higher motion amplitude and

This article has been accepted for publication in a future issue of this journal, but has not been fully edited. Content may change prior to final publication. Citation information: DOI 10.1109/JSEN.2019.2926189, IEEE Sensors Journal

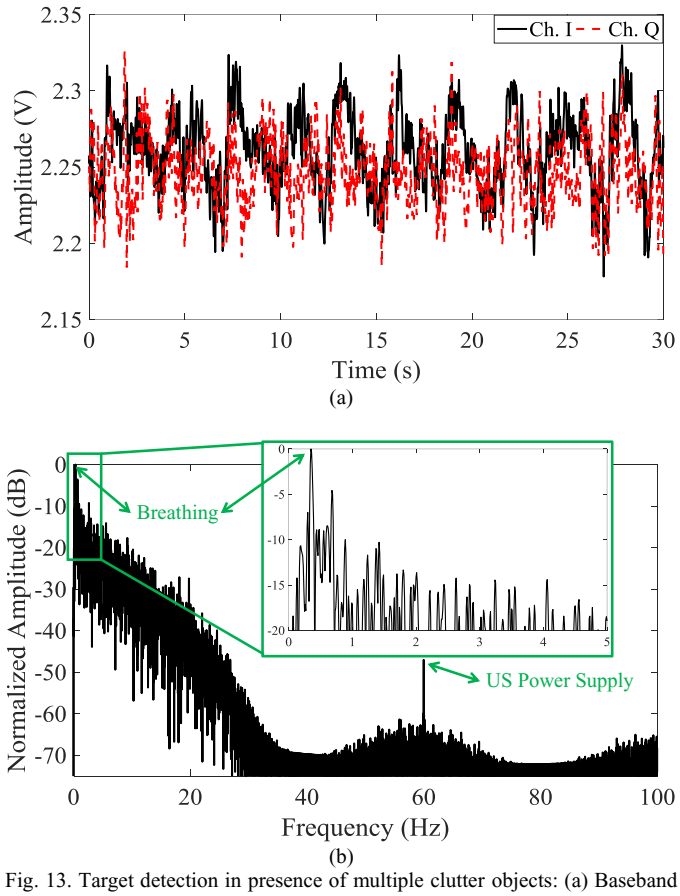

Fig. 13. Target detection in presence of multiple clutter objects: (a) Baseband output for tag and multiple clutter simultaneous motion (b) FFT of baseband signal.

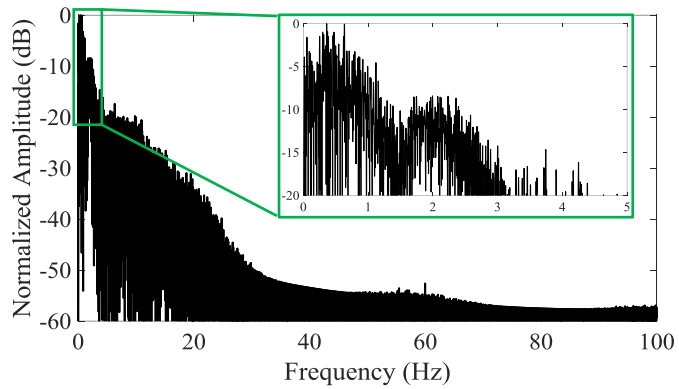

Fig. 14. FFT spectrum in presence of multiple clutter objects and no tag.

frequency. For the second experiment, the motion amplitude was set at 1 mm and motion frequency was set at 0.9 Hz. Fig. 10 shows the FFT result for this measurement. The FFT results for both 0.5 mm at 0.7 Hz and 1 mm at 0.9 Hz show that the tag motion led to a prominent peak at the corresponding motion frequency, while the copper plate did not cause any prominent peak above the noise floor.

B. Target Detection in Presence of a Single Clutter Object

The second experiment was performed to demonstrate motion discrimination when the small motion of the nonlinear tag and a large clutter motion coexist. Here the target i.e. person 1 wearing the tag was made to sit in front of the radar facing it and the other person was made to move back and forth in front of the radar. Person 2 was moving on a predefined track of length approximately 1.5 m and covered the distance in 2 seconds, so the speed was approximately 0.75 m/s. The Doppler shift f_{shift} due to person 2, measured using $f_{shift} = \frac{2 \cdot v_{source}}{\lambda}$, was 28 Hz. Here, the wavelength of the carrier at 5.74-GHz is λ, and v_{source} is the speed of person 2's movement. The measurement was performed, and baseband data was recorded using NI-USB 6009. The sampling frequency of the baseband data was set at 200 Hz to plot all frequencies up to 100 Hz.

Fig. 11(a) shows the baseband signal detected by the radar and its corresponding frequency spectrum is plotted in Fig. 11(b). The frequency spectrum shows no peaks due to clutter motion generated by person 2's movement. A peak at 60 Hz is the peak due to the US power supply. Although the clutter motion was larger than the tag motion, the radar was able to suppress the clutter motion. The intermodulation radar can successfully suppress clutter motion without the use of sophisticated hardware or any additional software-based approaches, such as those used in CW radars. Moreover, the setup was easy to install for real-time operation and avoids licensing issues. [3-6] The experiment was repeated with person 1 sitting in front of the radar not wearing the tag, while person 2 was moving. The baseband data was recorded and an FFT was performed. Fig. 12 shows the FFT result. From this graph, without the tag, breathing frequency cannot be determined, and the motion frequency of person 2 did not appear on the spectrum.

C. Target Detection in Presence of Multiple Clutter Objects

In [1], the CW radar was able to differentiate the clutter motion from the tag motion using a specialized hardware setup and prior calibration. Still, the radar was unable to distinguish multiple clutter objects from the target. In this experiment, person 1, wearing the tag, sat in front of the radar facing it to measure the breathing pattern while persons 2 and 3 moved back and forth in front of the radar. Persons 2 and 3 crossed each other in front of radar. The target was at 0.8 m away from the radar.

The data was recorded through NI-USB 6009 using LabVIEW. The sampling frequency of the measurement was 200 Hz. This was done to measure the clutter motion frequency that might be read by radar. The normal doppler frequency of a human walk at 5.8 GHz varies from 30-50 Hz. The baseband signal recorded by the radar is shown in Fig. 13(a). An FFT was performed on the baseband signal and is plotted in Fig. 13(b). From frequency spectrum it can be seen that the clutter motion generated by persons 2 and 3 was not present. The peak at 60 Hz is the frequency of the power supply in the US. The experiment was repeated for person 1 not wearing the tag, while person 2 and person 3 were moving around person 1. The baseband data was recorded and an FFT was performed on the data. Fig. 14 shows the frequency spectrum. A trend similar to Fig. 12 can be observed in Fig. 14. The breathing frequency was not observed, and the clutter did not appear in the frequency spectrum.

This article has been accepted for publication in a future issue of this journal, but has not been fully edited. Content may change prior to final publication. Citation information: DOI 10.1109/JSEN.2019.2926189, IEEE Sensors Journal

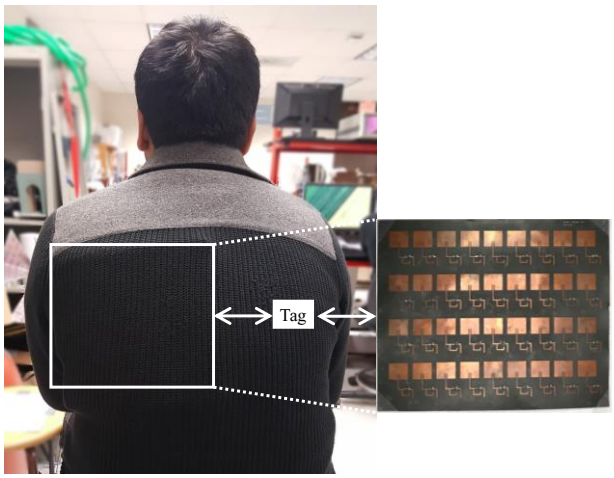

Fig. 15. Tag placement on person 1 for recording vital signs and tag in inset.

D. *Vital Sign Measurement*

The vital sign measurements of person 1 were performed at around 0.5 m away from the radar. Person 1 was sitting on the chair with their back facing the radar and the tag was fixed close to his heart. As heartbeats have lower motion amplitude relative to breathing, the tag was positioned to align with the heart with the purpose of capturing the weaker signal. The tag placement on person 1 is shown in Fig. 15. The normal breathing of person 1 varied from 0.3-Hz to 0.5-Hz. A reference measurement for the heartbeat came from a sensor fixed on the finger of person 1. The heartbeat reference was made up of piezoelectric material which converts a pulse signal into a voltage waveform, so that it can be recorded. The human pulse signal is the same as the heartbeat signal. The data from the radar and the reference were recorded using NI-USB 6009. The sampling frequency used to record the vital signs was set to 20 Hz. This was done as the vital signs of a human have a frequency below 10 Hz. After recording the data from the radar and the reference, an FFT was performed. The peak position of the heart was the same for both the reference and the radar. The baseband signal obtained by the radar is a one-dimensional array of voltages obtained with respect to time. A Short Time Fourier Transform (STFT) was performed. The baseband data was cut into smaller segments of equal size. An FFT was ~~is~~ performed on each segment and the Doppler shift due to target motion was plotted for each segment. An STFT graph is usually a combination of an FFT of each segment which depicts the frequency change over time. After comparing the FFT peaks, an STFT was done on the recorded data from the radar to validate the performance of the radar when measuring the vital signs. A Kaiser window with a size of 15 seconds and a step size of 0.5 seconds was used. Fig. 16(a) shows the baseband data recorded from the radar and the FFT is shown in Fig, 16(b). The STFT graph initially started at 7.5 seconds and ended at 27.5 seconds. In order to make the STFT graph start from 0 seconds, 7.5 seconds was deducted from the time, resulting in a range of 0 seconds to 20 seconds. The final STFT plot is shown in Fig. 16(c). [24]

IV. Conclusion

An intermodulation radar and a corresponding nonlinear tag were designed and experimentally tested with different targets. The receiver was able to amplify the 3rd-order frequency tone and attenuate the fundamental tones. The radar can successfully differentiate between the motions of a nonlinear tag from ~~a~~ large clutter. Compared to other nonlinear radars, the proposed intermodulation radar operates in the same frequency band to transmit and receive signals, which simplifies the hardware design and avoids licensing issues due to multiple-band operation. At the same time, this radar has a lower path loss and does not need active tags for operations. The future work is to make the radar portable by replacing signal generators with frequency synthesizers.

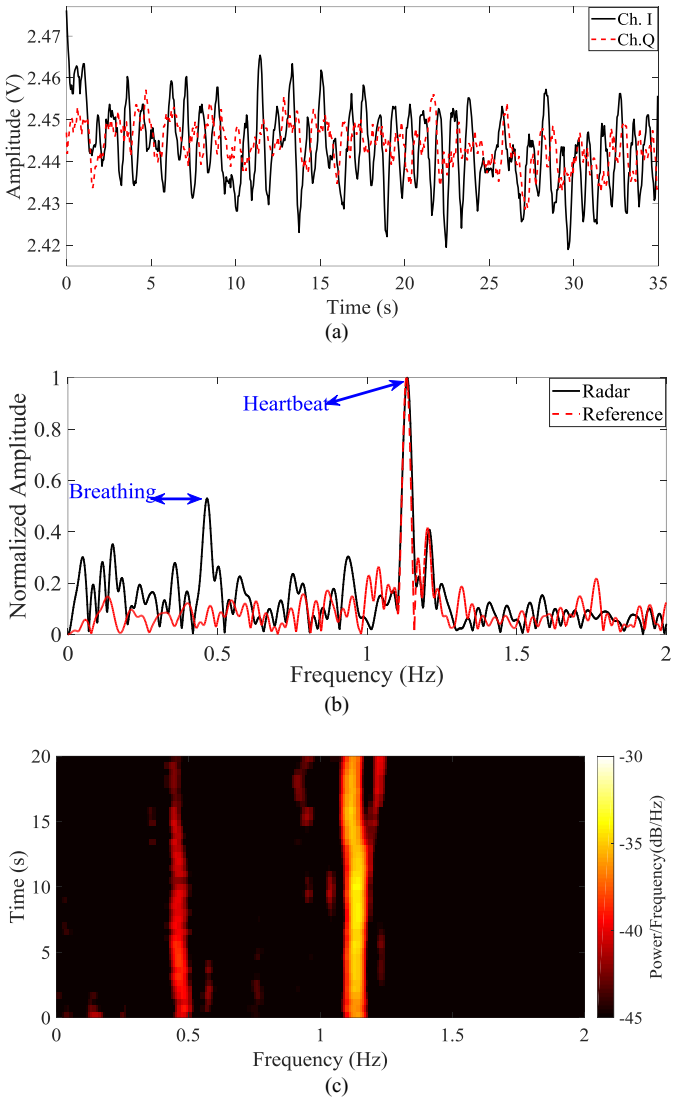

Fig. 16. Vital sign (a) Baseband signal from radar (b) FFT of the radar and reference signal (c) STFT of radar signal.

References

[1] T. J. Kao, Y. Yan, T. Shen, A. Y. Chen and J. Lin, "Design and Analysis of a 60-GHz CMOS Doppler Micro-Radar System-in-Package for Vital-

Sign and Vibration Detection," *IEEE Trans. Microw. Theory Techn.*, vol. 61, no. 4, pp. 1649-1659, April 2013.

[2] D. Rodriguez, and C. Li, "A Digital I/Q Correction Technique for a 125-GHz Interferometric Radar with Sub-Micrometer Sensitivity," *IEEE MTT-S Int.l Microw. Symp.*, 2019.

[3] M. Tang, F. Wang and T. Horng, "Single Self-Injection-Locked Radar With Two Antennas for Monitoring Vital Signs With Large Body Movement Cancellation," *IEEE Trans. Microw. Theory Techn.*, vol. 65, no. 12, pp. 5324-5333, Dec. 2017.

[4] S. Kazemi, A. Ghorbani, H. Amindavar, and C. Li, "Cyclostationary approach to Doppler radar heart and respiration rates monitoring with body motion cancelation using radar Doppler system," *Biomed. Signal Process. Control*, vol. 13, no. 4, pp. 79–88, Sep. 2014.

[5] Q. Lv, Y. Dong, Y. Sun, C. Li, and L. Ran, "Detection of bio-signals from body movement based on high-dynamic-range Doppler radar sensor," *IEEE MTT-S Int. Microw. Symp. Dig.*, Sep. 2015, pp. 88–89.

[6] S. Tomii and T. Ohtsuki, "Heartbeat detection by using Doppler radar with wavelet transform based on scale factor learning," *Proc. IEEE Int. Conf. Commun. (ICC),* Jun. 2015, pp. 483–488.

[7] C. Mandel, C. Schuster, B. Kubina, M. Schüßler and R. Jakoby, "Dual Frequency Selective Multiple Access With Quasi-Chipless/Powerless RFID Mixer Tags," *IEEE Microw. Wireless Compon. Lett.*, vol. 24, no. 8, pp. 572-574, Aug. 2014.

[8] K.A. Gallager, "Harmonic Radar: Theory and Applications to nonlinear target detection, tracking, imaging and classification", Ph.D. dissertation, The Pennsylvania State University, USA, Dec. 2015.

[9] Z. Tsai et al., "A High-Range-Accuracy and High-Sensitivity Harmonic Radar Using Pulse Pseudorandom Code for Bee Searching," *IEEE Trans. Microw. Theory Techn*., vol. 61, no. 1, pp. 666-675, Jan. 2013.

[10] A. Mishra and C. Li, "5.8-GHz ISM band intermodulation radar for high-sensitivity motion-sensing applications," *IEEE Radio and Wireless Symp.*, pp. 4-6, Jan. 2018.

[11] J. Raoult, A. Martorell, L. Chusseau and C. Carel, "Intermodulation Radar for RF Receiver Detections," *European Radar Conference,* 2018.

[12] W. D. Watson, "Improvements in the Suppression of External Nonlinearities ('Rusty Bolt' Effects) Which Affect Naval Radio Systems," *IEEE Int. Symp. on Electromagnetic Compatibility*, 1983, pp. 1-4.

[13] P. L. Lui, "Passive intermodulation interference in communication systems," *Elec. & Comm. Eng. J.*, vol. 2, no. 3, pp. 109-118, June 1990.

[14] J. Landt, E. Miller and F. Deadrick, "Time domain modeling of nonlinear loads," *IEEE Trans. Antennas Propagat.*, vol. 31, no. 1, pp. 121-126, January 1983.

[15] T. Sarkar and D. Weiner, "Scattering analysis of nonlinearly loaded antennas," *IEEE Trans. Antennas Propagat.*, vol. 24, no. 2, pp. 125-131, March 1976.

[16] A. Singh and V. M. Lubecke, "Respiratory Monitoring and Clutter Rejection Using a CW Doppler Radar with Passive RF Tags," *IEEE Sensors J.*, vol. 12, no. 3, pp. 558-565, March 2012.

[17] S. Shopov, M. G. Girma, J. Hasch, N. Cahoon and S. P. Voinigescu, "Ultralow-Power Radar Sensors for Ambient Sensing in the V -Band," *IEEE Trans. Microw. Theory Techn.*, vol. 65, no. 12, pp. 5401-5410, Dec. 2017

[18] N. El Agroudy, M. El-Shennawy, N. Joram and F. Ellinger, "Design of a 24 GHz FMCW radar system based on sub-harmonic generation" *IET Radar Sonar Navig*., vol. 12, no. 9, pp. 1052-1057, 9 2018.

[19] Resources.altium.com. (2019). The Advantages and Disadvantages of Active and Passive RFID Technologies. [online] Available at: https://resources.altium.com/pcb-design-blog/the-advantages-and-disadvantages-of-active-and-passive-rfid-technologies [Accessed 19 May 2019]

[20] M. S. Dadash, J. Hasch, P. Chevalier, A. Cathelin, N. Cahoon and S. P. Voinigescu, "Design of Low-Power Active Tags for Operation With 77–81-GHz FMCW Radar," *IEEE Trans. Microw. Theory Techn.,* vol. 65, no. 12, pp. 5377-5388, Dec. 2017.

[21] N. C. Kuo, B. Zhao and A. M. Niknejad, "A 10-Mb/s Uplink Utilizing Rectifier Third-Order Intermodulation in a Miniature CMOS Tag," *IEEE Microw. Wireless Compon. Lett*., vol. 27, no. 11, pp. 1031-1033, Nov. 2017.

[22] A. D. Droitcour, O. Boric-Lubecke, V. M. Lubecke, J. Lin and G. T. A. Kovacs, "Range correlation and I/Q performance benefits in single-chip silicon Doppler radars for noncontact cardiopulmonary monitoring," *IEEE Trans. Microw. Theory Techn*., vol. 52, no. 3, pp. 838-848, March 2004.

[23] Narayanan, Ram, et al. "Hardware Design of a High Dynamic Range Radio Frequency (RF) Harmonic Measurement System." *Instruments*, vol. 2, no. 3, 2018, p. 16.

[24] Y. Li, Z. Peng, R. Pal and C. Li, "Potential Active Shooter Detection Based on Radar Micro-Doppler and Range-Doppler Analysis Using Artificial Neural Network," in *IEEE Sensors Journal*, vol. 19, no. 3, pp. 1052-1063, Feb. 2019.

Ashish Mishra (S'15) received the B.E. degree in Electronics and Telecommunication Engineering from University of Mumbai and MS in Electrical Engineering from Texas Tech University in 2016. He is currently pursuing the Ph.D. degree in Electrical Engineering at Texas Tech University, Lubbock, TX, USA. His current research interests include microwave circuits, wireless RF sensors, and their biomedical applications.

Changzhi Li (S'06-M'09-SM'13) received the B.S. degree in electrical engineering from Zhejiang University, China, in 2004, and the Ph.D. degree in electrical engineering from the University of Florida, Gainesville, FL, in 2009.

In the summers of 2007–2009, he was first with Alereon inc. Ausitn, TX, USA and then Coherent Logix inc. Austin, TX, USA, where he was involved with ultrawideband (UWB) transceivers and software-defined radio, respectively. He joined Texas Tech University as an Assistant Professor in 2009 and became an Associate Professor in 2014. His research interests include biomedical applications of microwave technology, wireless sensors, and RF/analog circuits.

Dr. Li was a recipient of the IEEE Microwave Theory and Techniques Society (MTT-S) Outstanding Young Engineer Award, the IEEE Sensors Council Early Career Technical Achievement Award, the ASEE Frederick Emmons Terman Award, the IEEE-HKN Outstanding Young Professional Award, the NSF Faculty Early CAREER Award, and the IEEE MTT-S Graduate Fellowship Award. He is an Associate Editor of the IEEE TRANSACTIONS ON MICROWAVE THEORY AND TECHNIQUES, the IEEE TRANSACTIONS ON CIRCUITS AND SYSTEMS I, and the IEEE JOURNAL OF ELECTROMAGNETICS, RF AND MICROWAVES IN MEDICINE AND BIOLOGY. He served as an Associate Editor of the IEEE TRANSACTIONS ON CIRCUITS AND SYSTEMS II from 2014 to 2015. He served as a TPC Co-Chair for the IEEE MTT-S International Microwave Biomedical Conference from 2018 to 2019, and the IEEE Wireless and Microwave Technology Conference from 2012 to 2013.